Diamond films heteroepitaxially grown on platinum (111)

Takeshi Tachibana, Yoshihiro Yokota, Koichi Miyata, Takashi Onishi, and Koji Kobashi
Kobe Steel Ltd., Electronics and Information Technology Laboratory, 1-5-5 Takatsukadai, Nishi-ku, Kobe 651-22, Japan

Masayoshi Tarutani, Yoshizo Takai, and Ryuichi Shimizu
Department of Applied Physics, Osaka University, 2-1, Yamadaoka, Suita, Osaka 565, Japan

Yoshihiro Shintani
Department of Electrical and Electronic Engineering, The University of Tokushima, 2-1, Minamijosanjima, Tokushima 770, Japan
(Received 26 June 1997)

Diamond films were grown by microwave plasma chemical vapor deposition on *as-received* platinum (Pt) foils, specially processed Pt foils with (111) domains, bulk single-crystal Pt with a (111) surface, and single-crystal Pt(111) films deposited on strontium titanate (111). In all cases, the substrate surfaces had been significantly roughened by scratching to enhance diamond nucleation. Nevertheless, it was found by scanning electron microscopy that diamond films grown on the (111) areas of the above substrates had azimuthally aligned (111) faces, where a significant spontaneous coalescence developed between neighboring faces. An observation of the diamond-Pt interface region by transmission electron microscopy indicated that diamond crystals had an epitaxial relationship with Pt, and a (111) crystal at a diamond film surface contained an extremely low density of dislocations on the order of $10^8/cm^2$. Effects of H_2 and CH_4/H_2 plasma on a Pt surface, as well as the nucleation and growth process, were investigated in detail. [S0163-1829(97)01047-3]

I. INTRODUCTION

Heteroepitaxial growth of diamond by chemical vapor deposition (CVD) is one of the most important issues in diamond film research today. The latest finding in the field was obtained by one of the present authors (Y. S.):[1] diamond films with highly oriented and spontaneously coalesced (111) faces can be grown on the (111) surface of platinum Pt foil despite the fact that the Pt surface had been roughened by scratching with buff polishing and ultrasonic treatment. This method is referred to as the ''Shintani process'' after the name of the inventor.[2] The present work was motivated by Shintani's finding, and directed us to elucidate the nucleation and growth processes of these diamond films with their unique surface morphology.

Since the establishment of modern CVD methods of diamond growth at the National Institute for Research in Inorganic Materials (NIRIM),[3] attempts have been made to deposit single-crystal diamond films from the vapor phase. However, the surface free energy of diamond is so high that the two-dimensional growth of diamond on foreign substrates is very difficult. Furthermore, the covalent C-C bonds in diamond are so rigid that diamond nuclei, individually grown on a substrate, are very unlikely to coalesce without leaving grain boundaries between them, unless the diamond nuclei have been perfectly aligned with each other. However, it was shown that single-crystal diamond films can be heteroepitaxially grown on single-crystal cubic boron nitride (cBN),[4,5] because of the close match of lattice constants between the two materials (3.567 Å for diamond and 3.615 Å for cBN). Unfortunately, single-crystal cubic boron nitride is synthesized by the high-temperature–high-pressure method, which is similar to how the single-crystal diamond is produced, and therefore its surface is usually only less than a few mm^3.

A method of growing a highly oriented diamond film (HOD) was found by Stoner and Glass[6] using the bias-enhanced nucleation (BEN) technique created by Yugo *et al.*[7] to nucleate (100)-oriented diamond on pristine, unscratched β-SiC. Here, the diamond crystals on β-SiC were found to have an epitaxial relationship, diamond (100)$\|\beta$-SiC(100) and diamond $\langle 110\rangle \| \beta$-SiC $\langle 110\rangle$. More recently, (100)-oriented HOD films with totally coalesced (100) faces were demonstrated in Ref. 8 using the BEN technique for nucleation, followed by a (100) texture growth and a lateral growth. HOD films were also grown on Si(100) using the BEN technique.[9,10] In this case, the silicon surface is often carburized by hydrocarbon plasma before BEN to convert it to β-SiC. However, by means of polar x-ray diffraction (XRD), it was found that the coalesced HOD films were not single crystal, and an angular distribution of about $\pm 2.5°$ still remained among the diamond crystals.[11] Also, the existence of a small angular misalignment of about 5° between neighboring diamond crystals was revealed by transmission electron microscopy (TEM). This residual orientational disorder is considered to originate from the difference in the lattice constants between diamond and the substrates (4.348 Å for SiC and 5.431 Å for Si). (111)-oriented HOD films have also been grown on Si(111), but the degree of the orientational alignment of diamond crystals was not so good as that of the (100) HOD films on Si(100).[12]

It was reported that diamond crystals can be heteroepitaxially grown on single-crystal metal substrates such as nickel (Ni) and cobalt (Co).[13–15] These materials have lattice constants close to that of diamond (3.517 Å for Ni and 3.554 Å for Co). Unfortunately, it was only discrete and eroded diamond particles that resulted on these substrates due to

reactions of diamond with the metals in the high-temperature environment of diamond CVD.[13–15] Regarding diamond CVD on Pt, only a few studies have been done:[16–19] Belton and Schmieg[17,18] studied the surface chemistry of deposits on Pt at the initial stage of diamond CVD by x-ray photoelectron spectroscopy (XPS). It was found that graphitic carbon adsorbed at the Pt surface was first converted to hydrocarbons and then to diamond as the growth continued; Takaya and Sakamoto[19] observed by XPS that there was no chemical shift in the Pt($4f$) and C($1s$) bands, suggesting that no chemical reaction and compound formation took place between Pt and carbon. Neither of the above groups observed oriented growth of diamond on Pt substrates, nor was there any attempt of heteroepitaxial diamond growth on Pt, presumably because of the large difference in lattice constants between diamond and Pt (3.924 Å for Pt). Recently, however, Shintani and co-workers[1,2] were able to grow the aforementioned diamond films with the unique surface morphology on specially processed Pt foils with fairly large (111) domains at the surface. It was also confirmed that similar diamond films grew on both bulk single-crystal Pt(111) and single-crystal Pt(111) films sputter deposited on single crystal strontium titanate ($SrTiO_3$) (111).[20]

At this stage, it must be noted that the term ''heteroepitaxy'' as used for diamond growth usually includes both ''uniform'' heteroepitaxy such as the diamond growth on cBN and ''local'' heteroepitaxy such as the growth on β-SiC and Si. In the latter case, heteroepitaxy is imperfect and local because of the fairly large difference of lattice constants between diamond and the substrate materials. Even so, the term ''heteroepitaxy'' is widely used because azimuthally oriented, and in certain cases, entirely coalesced diamond films are grown on those substrates. In the present paper, ''heteroepitaxy'' is used in the latter sense.

In the present paper, a detailed study of diamond growth on Pt is described. The present paper consists of four studies: (i) effects of plasma treatment on the Pt surface; (ii) nucleation and growth of diamond on *as-received* Pt foils, specially processed Pt foils with (111) domains, bulk Pt(111) single crystals, and single crystal Pt films formed on $SrTiO_3$(111); (iii) characterization of the highly oriented, spontaneously coalesced diamond films by scanning electron microscopy (SEM), XRD, and Raman spectroscopy; and finally (iv) observation of interface and defect structures of the diamond films by planar and cross-sectional TEM. In Sec. II, experimental details are described. The results and discussion are presented in Sec. III, and the growth process is summarized in Sec. IV. Finally, the conclusion is given in Sec. V. It was found by polar XRD and TEM that (111)-oriented diamond crystals that have epitaxially nucleated on Pt(111) determine the coalesced (111) film morphology at a later stage as a result of growth competition with nonepitaxial diamond crystals.

II. EXPERIMENT

A. Sample preparation

The following four types of Pt substrates were used in the present study:

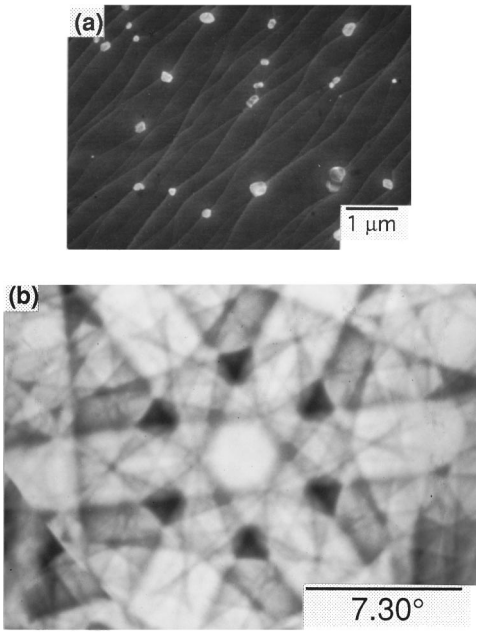

FIG. 1. (a) SEM micrograph and (b) ECP of a Pt(111) domain on the surface of specially processed Pt foil.

(1) As-received Pt foils: the thickness was 0.2 mm, and the foil surface consisted of randomly oriented crystal domains of about 1 μm^2.

(2) Specially processed Pt foils: as-received Pt foils of about 0.5-mm thickness were processed by the method created by Shintani[1] in the following manner: they were first thinned by a roller, and then annealed overnight in air at about 1500 °C. After the thinning-annealing process was repeated several times until the foil thickness became less than about 0.2 mm, the surface of the Pt foil contained many (111) domains of about 2500–10 000 μm^2. Figure 1(a) shows an SEM photograph of a Pt(111) domain taken from the surface normal of the foil. Although the foil had been subject to the thinning-annealing processes, the (111) surface had a wavy structure after annealing. The small particles seen in Fig. 1(a) were found to be Pt by Auger electron spectroscopy (AES), but the cause of the particle formation has not yet been identified. The (111) orientation of the domains was confirmed by electron channeling pattern (ECP), as shown in Fig. 1(b). The sixfold symmetry of the ECP pattern indicated that the (111) domain had a good crystallinity.

(3) Bulk Pt single crystals: the diameter and the thickness were 12 and 2 mm, respectively. The (111) orientation and its crystallinity were examined by XRD and ECP.

(4) Single-crystal Pt(111) films deposited on $SrTiO_3$(111): Pt(111) films were deposited by magnetron sputtering on single crystal $SrTiO_3$(111) of 5 mm square in surface area and 0.5 mm in thickness. The deposition rate of Pt was about 2.5 nm/s. Subsequently, they were annealed at 1000 °C for 5 h in a vacuum of 10^{-7} Torr. The films were examined by XRD and ECP, and found to have the same quality as the bulk single crystal.

Except for the Pt films, the substrates were buff polished using a 0.25-μm diamond powder. All the Pt substrates were ultrasonically abraded in diamond powder-suspended ethanol, where the powder size was 15–30 μm. Consequently,

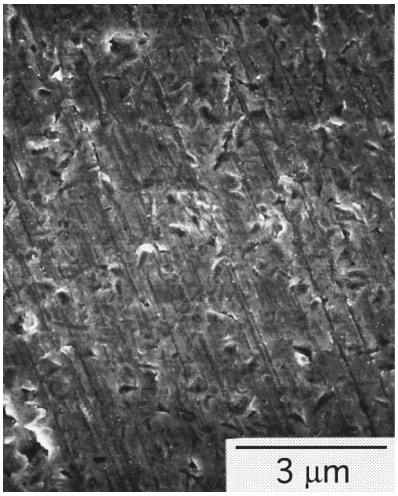

FIG. 2. A SEM micrograph of a bulk single crystal Pt(111) surface after the ultrasonic treatment.

the substrate surfaces were extremely roughened, as seen in Fig. 2. Finally, they were ultrasonically rinsed in acetone and ethanol.

B. Plasma treatment of Pt

In order to study the behavior of Pt surface in plasma environments, as-received Pt foils and bulk single-crystal Pt were exposed to (a) pure H_2 plasma, or (b) 0.5% CH_4/H_2 plasma using the NIRIM-type microwave plasma CVD reactor shown in Fig. 3. In these treatments, the gas pressure was 50 Torr (1 Torr=133 Pa), and the substrate temperature (T_s), measured by an optical pyrometer assuming that the emissivity was unity, was kept at 800 °C for 1–60 min. As a reference, the bulk single-crystal Pt samples were (c) annealed at 800 °C in vacuum. The sample surfaces were then investigated by AES.

C. Diamond nucleation and growth

Diamond growth was carried out using the same reactor. The substrate was held on either a quartz or a Mo holder. For a survey of proper growth conditions, T_s was set at a temperature between 770 and 920 °C by controlling the microwave power. The source gas used was a CH_4/H_2 mixture with a CH_4 concentration $c_M=0.2-1.2$ %, the gas pressure was 50 Torr, and the input microwave power was 350–400 W. The growth rate of diamond under these conditions was 0.2–0.3 μm/h. On the basis of on these experiments, $c_M=0.3\%$ and $T_s=875$ °C were chosen as the standard CVD conditions, for the reasons described in Sec. III E.

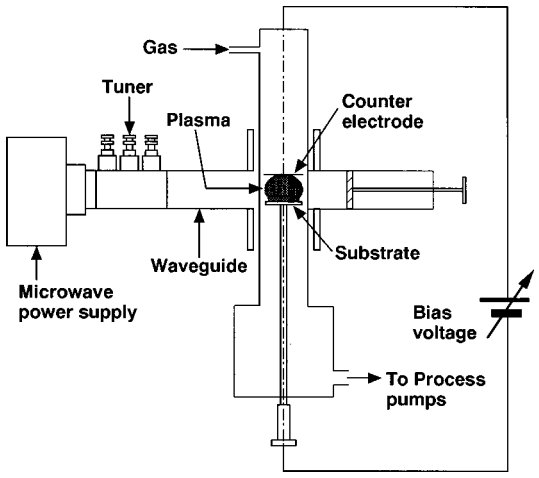

FIG. 3. A schematic diagram of the NIRIM-type microwave plasma CVD reactor.

For the nucleation study, diamond CVD was done using the standard CVD conditions for 1–15 min on as-received Pt foils that had been pretreated by the methods described in Sec. I. In addition, the BEN technique[7] was used. In this case, the substrate, placed in the reactor, was negatively biased (−150 to −250 V) against a grounded wire electrode that was placed above the plasma, as shown in Fig. 3. The substrate bias was applied for 10–60 min in a plasma of $c_M=2-10\%$. According to separate experiments using Si as a substrate,[10] these biasing conditions induced a diamond nucleation of $1\times10^8-5\times10^9$ cm^{-2}. Diamond growth was subsequently carried out on these samples for 1–15 min using the standard CVD conditions.

The time evolution of the film morphology was investigated using the standard CVD conditions on bulk single-crystal Pt(111) by interrupting CVD at certain time intervals. In the first series of experiments, the interruption was after every 10 min from the start, and, in the second series, it was after 1, 2, 3, 5, and 10 h from the start. In both cases, the same positions on the specimens were observed by SEM.

D. Film characterization

Field-emission SEM was used to observe the surface morphology of the films. Raman spectroscopy was done to observe the film quality, using an SPEX 1877 TRIPLEMATE with a multichannel analyzer, where the light source was a 4-mW Ar laser at 514.5 nm. Standard $\theta-2\theta$ XRD scans were carried out using a powder diffractometer with the Cu K_α radiation. Polar XRD was undertaken to observe the orientational structure of the diamond films as well as the Pt substrates in a Schultz reflection configuration, where a $\frac{1}{6}$ mm slit was placed at about 200 mm from the sample. The detector position was fixed at $2\theta=43.9°$ for diamond (111) diffraction and at $2\theta=39.9°$ for Pt(111) diffraction, and the tilt and azimuthal angles were scanned in the ranges of $15° \leqslant \chi \leqslant 90°$ and $0° \leqslant \phi \leqslant 360°$, respectively.

E. TEM observation

The observation by TEM and transmission electron diffraction (TED) was done by JEOL-200CX at an acceleration voltage of 200 kV. The specimens for TEM were prepared using a gallium (Ga) focused-ion beam (FIB) system of Eiko Engineering, i.e., ''Nanotome'' (Ref. 21) at an acceleration voltage of 25 kV. The sampling positions are illustrated in Fig. 4. For planar TEM observations, areas of about 100 μm^2 were horizontally carved out of three regions from a delaminated, 10-μm-thick diamond film grown on bulk single-crystal Pt(111): a diamond-Pt interfacial region, a central region, and a surface region.

For cross-sectional TEM observations, a 9-μm-thick diamond film grown on a single-crystal Pt(111) film was cleaved into small pieces, and a delaminated diamond piece

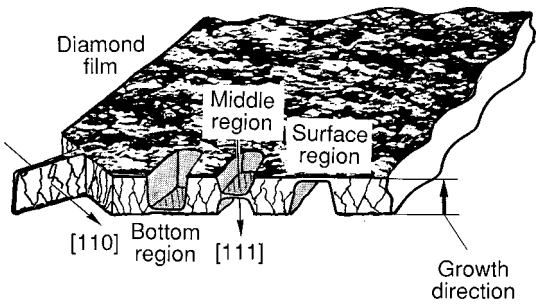

FIG. 4. A schematic diagram showing the location of the TEM specimen.

was vertically carved out by FIB along the ⟨110⟩ direction to form a thin section about 10 μm wide. Also, the center of a (111) diamond face at the surface was vertically cut out of the 10-μm-thick diamond film for a cross-sectional TEM observation.

III. RESULTS AND DISCUSSION

A. Pt surfaces in plasma environments

As described in Sec. I, azimuthally oriented diamond grains are spontaneously grown on initially scratched Pt(111) surfaces. To elucidate the cause of this curious phenomenon, the change in the structure of the Pt surface in H_2 and CH_4/H_2 plasma was investigated.

Figure 5(a) is the XRD spectrum of as-received Pt(111), where minor diffraction peaks of Pt from (200), (220), (311), (400), and (331) are detected in addition to the major diffraction peaks of (111) and (222) at $2\theta = 39.9°$ and 75.3°, respectively. Figure 5(b) is the XRD result after the Pt surface was scratched by the ultrasonic treatment, where the minor peaks are significantly weak. Notice that diamond (111) diffraction is present, indicating that diamond powder was embedded in Pt due to the ultrasonic treatment. The corresponding SEM micrographs of the as-received and ultrasonically scratched Pt surfaces are shown in Figs. 6(a) and 6(b). It is

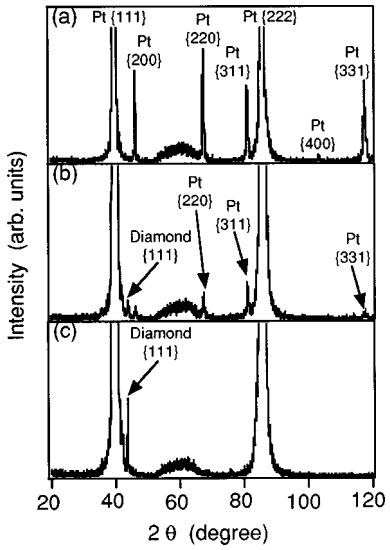

FIG. 5. X-ray diffraction of single-crystal Pt(111); (a) as received, (b) after ultrasonic treatment, and (c) after exposure to H_2 plasma.

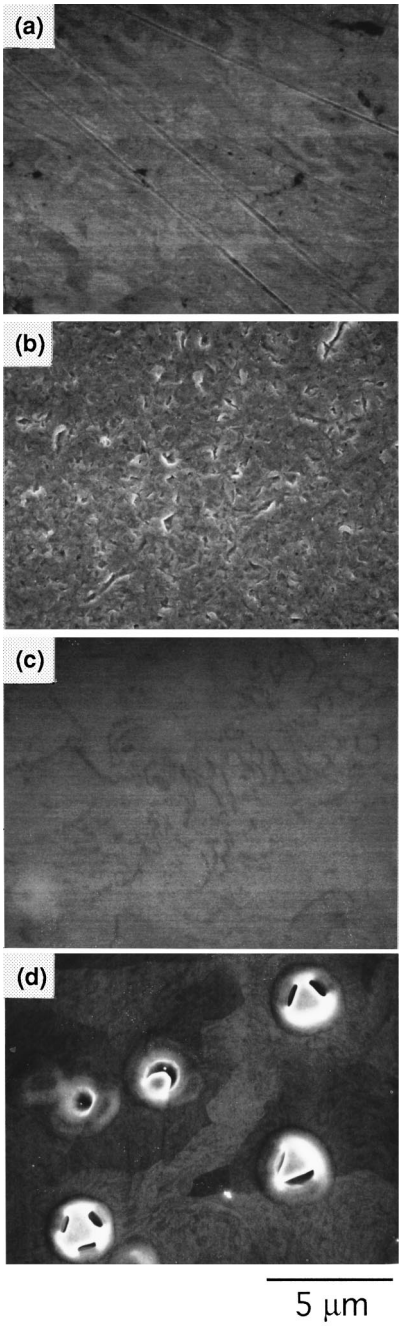

FIG. 6. (111) surface of bulk single-crystal Pt: (a) as-received surface, (b) ultrasonically scratched surface, (c) after exposure to H_2 plasma at 800 °C for 1 min, and (d) after exposure to 0.5% CH_4/H_2 plasma at 800 °C for 60 min.

noted that no diamond particles are observed by SEM on the scratched Pt surface, although they are detected by XRD.

Figure 6(c) shows a SEM micrograph of the Pt surface after an exposure to H_2 plasma for 1 min. It shows clearly that the scratches and dimples on the initial surface have completely disappeared to create a smooth surface. In the corresponding XRD of Fig. 5(c), only the major diffraction lines of Pt(111) and (222) are observed, while the minor diffraction lines disappear, which indicates that the single-crystal quality of Pt was improved over the as-received material by the plasma treatment. This is in good contrast to the result of the reference experiment in which the XRD pattern

was unchanged by the vacuum annealing at 800 °C up to 60 min. These results indicate that H_2 plasma played an important role in the structural recovery of the Pt(111) surface. It therefore follows that, in diamond CVD, the single-crystal Pt(111) domains or surfaces that had once been roughened by the scratching were quickly smoothed, and the (111) surface structure was recovered shortly after the CVD started.

In Fig. 5(c), diamond (111) is more clearly visible for the H_2 plasma-treated Pt surface. This implies that the residual diamond powder embedded in Pt was preferentially oriented toward (111) during the H_2 plasma treatment and the structural recovery of Pt(111) surface. The growth of azimuthally oriented diamond film on scratched surface is not characteristic of Pt, because it has also been achieved on scratched surfaces of Ni and Co substrates.[13–15] However, unlike Pt these metals are known to react strongly with diamond, so that the nucleation mechanism of diamond on Pt is assumed to be different from that on Ni and Co.

Figure 6(d) shows a SEM micrograph of the Pt(111) surface treated by 0.5% CH_4/H_2 plasma. Unlike Fig. 6(c), a number of small voids were created on the surface. Those voids had threefold symmetry due to the symmetry of the Pt(111) surface. Since such voids were absent on the H_2 plasma-treated Pt surface, they are supposed to be formed by unspecified reactions of carbonatious molecular species with Pt. According to AES, it was found that the sp^2 carbon content was about 60% in the void area, while it was only about 35% in other areas. At the present stage, it is not known how the voids are formed, and why carbon content is higher in the void areas. It can only be speculated that carbon was absorbed either on the Pt surface or in the Pt bulk, and diffused to form carbon aggregates in the void areas in the CH_4/H_2 plasma environment.

B. Nucleation stage on Pt surface

In this section, nucleation of diamond is studied using as-received Pt foils as the substrates. Figures 7(a) and 7(c) are SEM micrographs of the surfaces after buff polishing and ultrasonic treatment, respectively, and Figs. 7(b) and 7(d) are the corresponding surfaces after diamond CVD for 1 min. It is seen that the nucleation density on the ultrasonically treated substrate [Fig. 7(b)] is about 7×10^8 cm^{-2}, one order of magnitude greater than the value of 4×10^7 cm^{-2} for the buff-polished Pt substrate [Fig. 7(d)]. Notice the difference in scales of SEM micrographs between Figs. 7(b) and 7(d). In order to further see the effect of biasing on nucleation, an as-received Pt foil was treated by the BEN technique, and subsequently, diamond CVD was carried out for 15 min. Figures 7(e) and 7(f) show the Pt surface after BEN and CVD, respectively. It is seen that the nucleation density is only about 2×10^5 cm^{-2}, which is similar to the value for untreated as-received Pt foil, although the BEN conditions were not optimized for Pt substrates. This result is in strong contrast to the BEN results on Si or SiC,[6–11] where a nucleation density of about 10^{10} cm^{-2} has been achieved. In Figs. 7(e) and 7(f), numerous voids and dark spots are seen on the Pt surface. According to AES, sp^2 carbon was included in them as in the films grown on single-crystal bulk Pt exposed to CH_4/H_2 plasma [see Fig. 6(d)].

Figures 7(a) and 7(b) show that no diamond crystals were formed along the scratch lines on Pt, unlike the phenomenon often seen for Si. Furthermore, according to a separate experiment in which as-received Pt was buff polished using an Al_2O_3 powder of 1 μm in size, and diamond CVD was subsequently done for 60 min under the same CVD conditions, the nucleation density was about 4×10^7 cm^{-2}. These two results seem to indicate that the nucleation density of about 4×10^7 cm^{-2} can be attributed to surface scratches created by the buff-polishing. If this is the case, the higher nucleation density of about 7×10^8 cm^{-2} on the ultrasonically treated substrate [Fig. 7(d)] is at least partly attributable to residual diamond particles embedded in the Pt surface during the ultrasonic pretreatment, which were detected by XRD (see Fig. 5).[22]

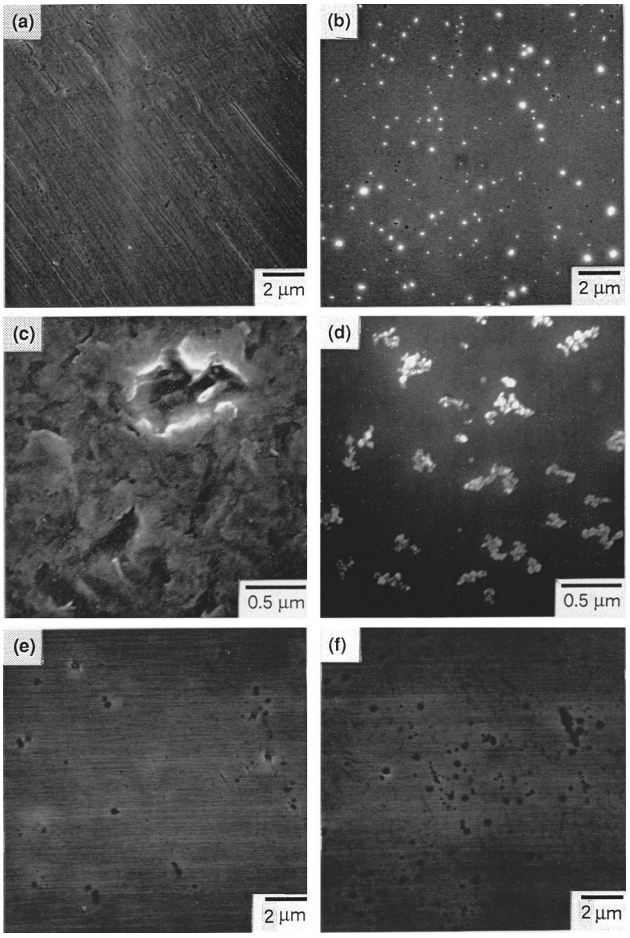

FIG. 7. Pt surfaces (a) buff polished using diamond paste, (b) after 1-min growth of diamond on (a), (c) ultrasonically treated; (d) after 1-min growth of diamond on (c), (e) after BEN, and (f) after 15-min growth of diamond on (e).

C. Initial growth stage

In order to study the initial stage of diamond growth after nucleation on bulk single-crystal Pt(111), diamond CVD was interrupted after (a) 20 min, (b) 30 min, (c) 45 min, (d) 60 min, (e) 75 min, and (f) 105 min from the start, and the same spot on the sample was observed by SEM. The results are presented in Figs. 8(a)–8(f), respectively. The first interesting feature seen in these micrographs is the occurrence of ''dissolution and recrystallization'' of diamond crystals on the Pt surface. For instance, the diamond crystal A is seen to

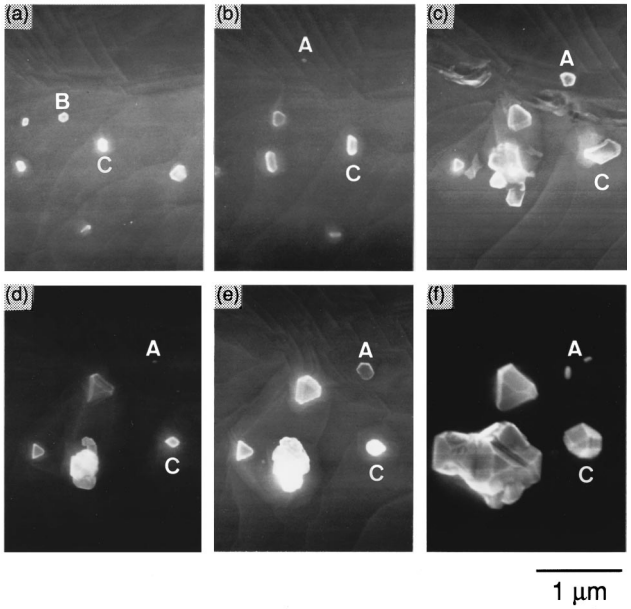

FIG. 8. SEM micrographs of diamond crystals grown on bulk single-crystal Pt(111) for (a) 20 min, (b) 30 min, (c) 45 min, (d) 60 min, (e) 75 min, and (f) 105 min.

repeatedly undergo this process in the micrographs: it is not visible on the surface in Fig. 8(a), and only vaguely seen in Fig. 8(b). It then emerges on the Pt surface in Fig. 8(c), but becomes a tiny particle in Fig. 8(d). In Fig. 8(e), crystal A appears as a well-faceted particle, but then splits into two particles in Fig. 8(f). On the other hand, crystal B, seen in Fig. 8(a), has disappeared in Fig. 8(b), and is not seen in the other micrographs. The second feature is the positional change of the diamond crystals, which is recognized as the change in the relative distances between the crystals in Figs. 8(a)–8(f). The third feature is that some crystals underwent rotations: for instance, crystal C changed its orientation markedly between Figs. 8(b) and 8(c). The positional and orientational changes of small diamond crystals on a Pt surface have been observed previously by Ishikura *et al.*[23] According to Reiss,[24] atomic clusters can translate or rotate to take an epitaxial alignment with respect to the substrate lattice under certain conditions. In the present work, it is likely that the molten Pt surface in plasma facilitated such motions.

The occurrence of ''dissolution and recrystallization'' of diamond crystals on the Pt substrate has not been reported before to our knowledge. Since the melting point of Pt (1772 °C) is much higher than the CVD temperature (875 °C), and the solid solubility of C in Pt is less than 1 at % at 875 °C according to the Pt-C binary phase diagram,[25] it is likely that a Pt-C-H ternary system plays an important role for the molten substrate surface. Indeed, Roy, Dewan, and Ravindranathan[26] reported a recrystallization of diamond from Ni-C and Cu-C solutions in H_2 plasma due to a metal-C-H complex formation. The SEM micrographs shown in Figs. 8(a)–8(f) indicate that the epitaxial growth of diamond described in the present paper resulted from the physical motion (positional and orientational changes) and chemical interaction (''dissolution and recrystallization'') of small diamond crystals at the Pt surface. The ''dissolution and recrystallization'' are also consistent with the intricate interface structure explained later in Sec. III H.

D. SEM observation of the growth process

Figures 9(a)–9(e) show the results of time evolution of the diamond growth on bulk single-crystal Pt(111). After 1 h [Fig. 9(a)], (110)- and (100)-oriented crystals, indicated by A and B, respectively, are clearly visible. After 2 h [Fig. 9(b)], (111)-oriented crystals indicated by C and D are seen to have grown faster than crystals A and B. After 3 h [Fig. 9(c)], the substrate surface is almost entirely covered with diamond crystals to begin a vertical growth. After 5 h [Fig. 9(d)], crystals C and D become larger than other crystals such as crystal B, and, after 10 h [Fig. 9(e)], crystal C grows over crystal B. The (110)-oriented crystal A still survived in Fig.

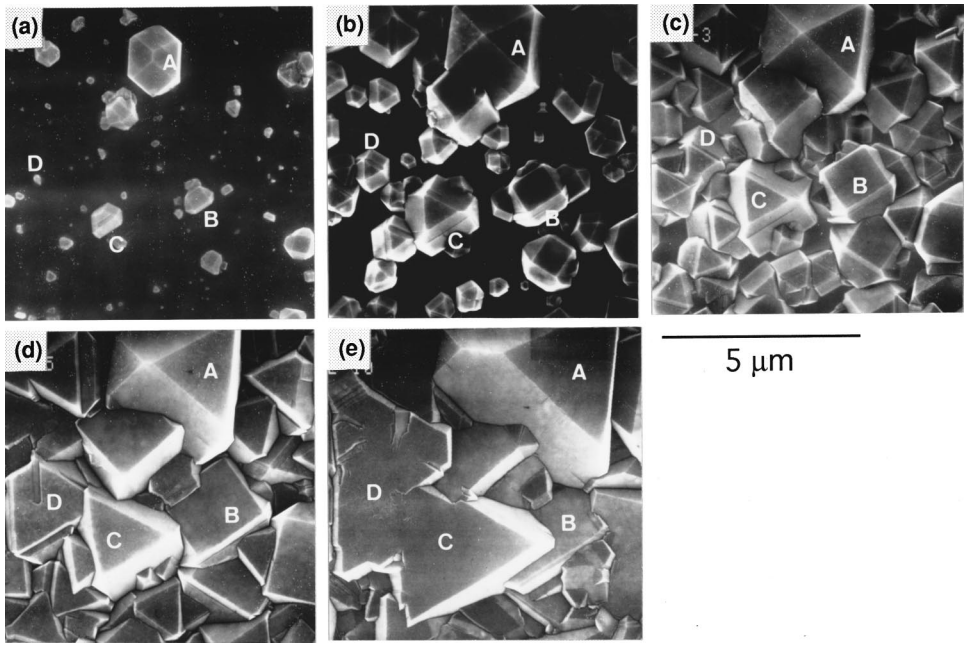

FIG. 9. SEM micrographs of diamond grown on bulk single-crystal Pt(111) for (a) 1 h, (b) 2 h, (c) 3 h, (d) 5 h, and (e) 10 h.

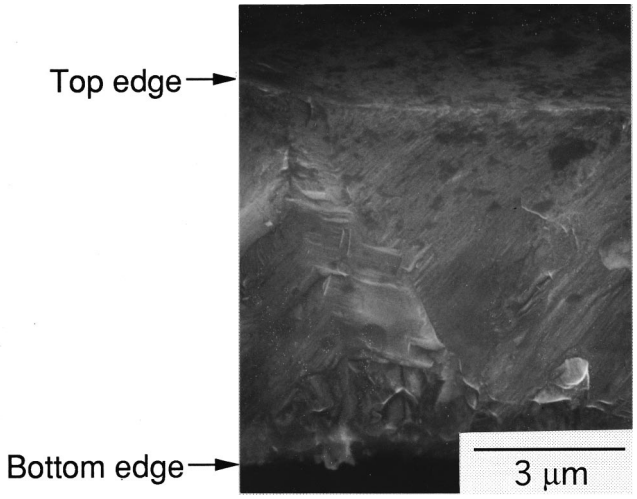

FIG. 10. Cross-sectional view of a diamond film grown for 30 h on bulk single-crystal Pt(111).

9(e) because of its high growth rate, but as will be seen later in Figs. 13–15, (111)-oriented crystals are totally dominant after 30 h. A remarkable feature in Fig. 9(e) is the occurrence of the coalescence between adjacent (111) faces of crystals C and D, implying that those crystals are azimuthally well aligned.

Figure 10 shows a fractured edge of a delaminated diamond film grown on bulk single-crystal Pt(111) for 30 h. It is seen that a (111)-oriented crystal grew up toward the film surface, suppressing the growth of adjacent crystals. It is also seen that the bottom of the diamond film is extremely rough. Since the Pt surface became smooth immediately after being immersed in plasma, this roughness is attributed to a unique nucleation process of diamond, which will be described later.

The results in Figs. 9 and 10 show that the (111)-oriented diamond films are completed by the growth competition known as the van der Drift texture evolution mechanism,[27] i.e., diamond crystals with (111) faces grow faster than other crystals, and consequently determine the film surface morphology. It was further observed that even though there were diamond crystals that had (111) faces, they were also taken over by azimuthally oriented diamond crystals with (111) faces more parallel to the substrate surface. It is known that given the growth conditions such as c_M and T_s, the surface morphology[28] of a CVD diamond film is determined by the fastest growth direction, and the growth morphology is quantitatively expressed using a ''growth parameter'' α defined by $\alpha=\sqrt{3}\ (\nu_{100}/\nu_{111})$, where ν_{100} and ν_{111} are the growth rates normal to (100) and (111) faces, respectively.[29] The range of the α parameter value is $1\leqslant\alpha\leqslant 3$, where $\alpha=1$ and 3 corresponds to regular octahedron and cube, respectively, and the intermediate values express cubo-octahedrons. The value of the α parameter can be estimated from the shape of diamond crystals grown under given CVD conditions. It appears that the condition of $\alpha\sim 1$ is satisfied in the results of Figs. 9 and 10, as diamond underwent stable (111) growth on Pt(111). This result is in contrast with that obtained by Barrat and Bauer-Grosse,[30] where (111) growth of diamond on the Si substrate is unstable and easily taken over by (110) growth, because it is difficult to maintain the $\alpha\sim 1$ condition on Si. Thus it is concluded that (i) a considerable number of epitaxially oriented diamond particles are formed on Pt(111), although nonepitaxial particles coexist in the early stage of CVD, and (ii) under proper CVD conditions, the growth conditions represented by $\alpha\sim 1$ are stably realized on Pt. Although the real cause for the experimental observation of the stable (111) growth is yet to be elucidated, it is assumed that the difference between Pt and Si arises from the catalytic action of Pt to hydrogen and hydrocarbons at elevated temperatures,[31] and the Pt-C-H complex formation mentioned in Sec. III C.

E. Surface morphology of diamond films grown on as-received Pt foils

Before going into the details of the oriented diamond film growth on (111) domains or surfaces of Pt, the results on the survey of appropriate CVD conditions are presented in this section. As described in Sec. III E, the growth parameter must be $\alpha\sim 1$ to obtain (111)-oriented films, and it is known that this requires high T_s and low c_M in CVD. Using this theory as a guide, diamond films were deposited for 5 h using different parameter values for c_M and T_s on as-received Pt foils.

Figure 11 shows the results at $T_s=875\,^{\circ}\mathrm{C}$. For $c_M=0.2\%$, no diamond growth was observed. For $c_M=0.3\%$ [Fig. 11(a)], most diamond crystals have (111) faces that are oriented parallel to the substrate. For $c_M=0.5\%$ [Fig. 11(b)], the (111) faces are overlapped by small crystallites due to secondary nucleation. For $c_M=0.8\%$ [Fig. 11(c)], the film surface consists of smaller and numerously twinned diamond crystals. Finally, for $c_M=1.2\%$ [Fig. 11(d)], the film becomes microcrystalline. It is thus confirmed that the surface morphology is strongly influenced by c_M. The surface morphology was also investigated in a separate series of growth experiments (the details are not described here) by varying T_s within the range of 770 and 920 °C, using $c_M=0.3\%$ as well as other values. However, it was found that the film morphology depended only weakly on T_s. From a closer examination of the SEM micrographs of the synthesized diamond films, it was concluded that, for $T_s=875\,^{\circ}\mathrm{C}$, the (111) faces developed most markedly, and were more parallel to the substrate surface. Hence, the growth conditions of $c_M=0.3\%$ and $T_s=875\,^{\circ}\mathrm{C}$ were selected as the standard CVD conditions for diamond synthesis. Figure 12 shows a SEM micrograph of a diamond film deposited for 30 h on an as-received Pt foil using standard CVD conditions. The film surface consists of (111) faces, and although the Pt substrate is polycrystalline, many (111) faces are oriented upward, presumably as a result of growth competition. However, their azimuthal orientations are random.

During these experiments, it was found by SEM that there were diamond crystals that were partially embedded in Pt near the peripheral of the substrate, as seen in Fig. 13. Here, the diamond CVD was done for 5 h using the standard growth conditions. This micrograph seems to indicate that the diamond nucleation took place beneath the Pt surface. If this is the case, it is likely that the nucleation center could be the diamond particles that were buried in Pt during the ultrasonic treatment. It is also inferred that a Pt-C-H complex

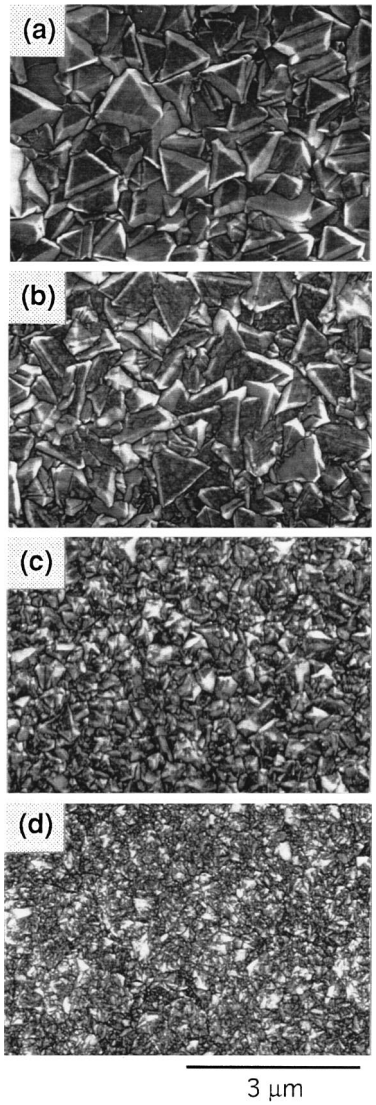

FIG. 11. SEM micrographs of diamond films grown on as-received Pt foils for c_M=(a) 0.3%, (b) 0.5%, (c) 0.8%, and (d) 1.2% at T_s=875 °C.

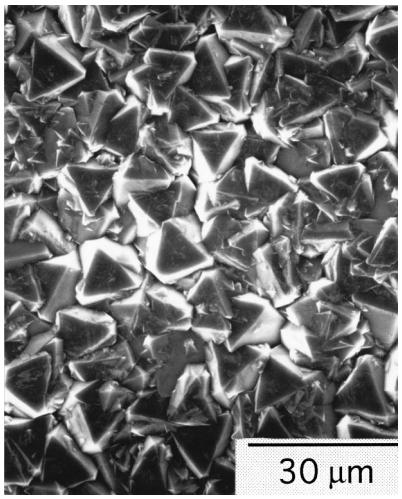

FIG. 12. SEM micrograph of a diamond film grown on as-received Pt foils for 30 h using c_M=0.3% and T_s=875 °C.

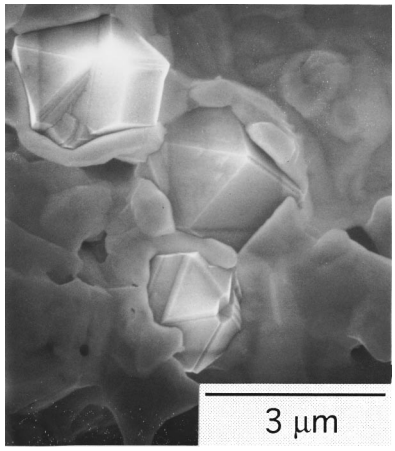

FIG. 13. Diamond crystals embedded in as-received Pt foil substrate.

formation plays a certain role for the nucleation and growth processes of the diamond crystals, in consistent with the results described in Sec. III C.

F. Oriented growth

Figure 14 shows a SEM micrograph of a diamond film grown for 50 h on a specially processed Pt foil. On the right-hand side of the figure, a large diamond crystal of approximately 10^4 μm^2 is seen. This crystal was formed as a result of a coalescence of smaller diamond crystals of 5–10 μm in size, and the grain boundaries on the surface were not apparent under SEM. It was found by ECP that the Pt domain under the large diamond crystal was (111). On the other hand, the left-hand side of Fig. 14 consists of randomly oriented diamond crystals with (111) faces dominant. In this case, the underlying Pt domains were not (111), but in unspecified orientations.

Figures 15(a) and 15(b) are SEM micrographs of diamond films grown for 30 and 40 h, respectively, on bulk single-crystal Pt(111). It is apparent from Fig. 15(a) that the film surface consists of azimuthally oriented (111) faces of diamond. Most of the oriented faces have coalesced to form a single ''network'' of (111) faces, while the rest of the region contains randomly oriented diamond crystals. This morphology was uniform over the entire substrate surface of 12 mm in diameter except for the very edge. In Fig. 15(b), the coalescence developed further from Fig. 15(a), while the randomly oriented area decreased, clearly indicating the possi-

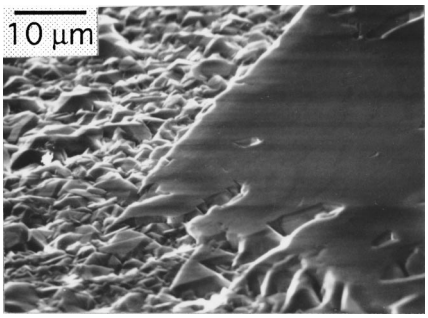

FIG. 14. SEM micrograph of a diamond film grown on a specially processed Pt foil.

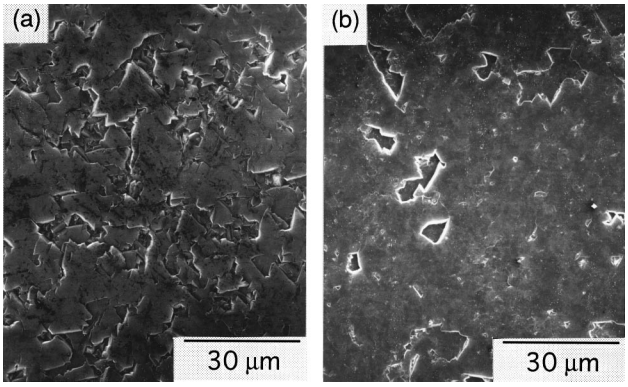

FIG. 15. SEM micrographs of diamond films grown for (a) 30 and (b) 40 h on bulk single-crystal Pt(111).

bility of forming a totally coalesced (111)-oriented diamond film on bulk single-crystal Pt(111).

Figure 16 shows a SEM micrograph of a diamond film grown for 30 h on an 8-μm-thick single-crystal Pt(111) film sputter deposited on an $SrTiO_3$(111) substrate. The film surface consists of (111) faces, and a coalescence is developed between neighboring (111) faces. Unlike the results of Figs. 15(a) and 15(b), the film surface is granular rather than planar, presumably due to the difference in the substrate material and uncontrollable growth conditions. From the results presented so far, it is concluded that azimuthally oriented diamond films are formed only on Pt(111) surface, if proper CVD conditions are used.

G. Film characterization

Figure 17 shows a Raman spectrum of a diamond film grown for 30 h on bulk single-crystal Pt(111) [see Fig. 15(a)], with a spectrum of a natural diamond as a reference. The main peak of the diamond film is located at 1339 cm^{-1}, a 7-cm^{-1} upward shift from the 1332-cm^{-1} band of the natural diamond. From this shift, the film stress was evaluated[32–35] to be compressive, and to have the value of 2.4 GPa, assuming that the compressive stress was hydrostatic. Furthermore, the intrinsic stress (σ_i) in the film was evaluated to be negative (tensile) using the following assumptions: the residual stress ($\sigma_{res}=2.4$ GPa) in the film was assumed to be $\sigma_{res}=\sigma_{th}+\sigma_i$, the sum of thermal stress (σ_{th}) and σ_i. The thermal stress is given by $\sigma_{th}=k(\alpha_s-\alpha_f)\delta T$, where k is the biaxial Young's modulus of the film (1230 GPa for diamond[36,37]), α_f and α_s are the thermal expansion

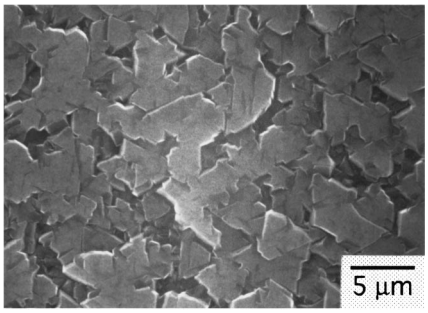

FIG. 16. SEM micrograph of a diamond film grown for 30 h on a single-crystal Pt(111) film sputter deposited on $SrTiO_3$(111).

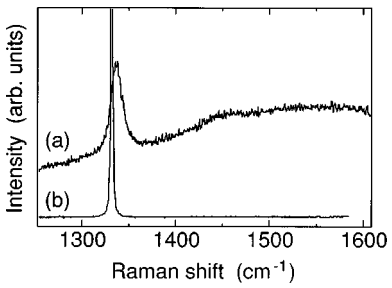

FIG. 17. Raman spectrum of a diamond film grown for 30 h on bulk single-crystal Pt(111). A spectrum of a natural single-crystal diamond is also shown for reference.

coefficients of diamond ($\alpha_f=4.7\times10^{-6}$/K) and Pt($\alpha_s=9.1\times10^{-6}$/K), respectively, and $\delta T(=850\ ^\circ C)$ is the difference between the growth temperature and room temperature. Accordingly, the thermal stress was calculated to be $\sigma_{th}=4.6$ GPa, and hence the intrinsic stress in the diamond film was tensile and -2.2 GPa.

In Fig. 17, the full width at half maximum (FWHM) of the main peak is about 12 cm^{-1} for the diamond film, while it is only 3 cm^{-1} for the natural diamond. The large FWHM of the diamond film is attributed to a nonuniform distribution of internal stress and a high density of defects in the film.[38,39] There is no appreciable band at about 1350 cm^{-1} due to the presence of sp^2 bonds, which indicates that nondiamond carbon is not included in the film to an appreciable amount. However, the high background indicates the existence of crystal defects in the film.

Figures 18(a) and 18(b) show the $\theta-2\theta$ x-ray-diffraction patterns of the diamond films grown for 5 and 30 h, respectively, on bulk single-crystal Pt(111). It consists of Pt(111) and Pt(222) diffractions at $2\theta=39.9°$ and 85.9°, respectively, and diamond (111) diffraction at $2\theta=43.9°$. Other allowed diffractions from diamond such as (220) at 74.5°, (311) at 91.5°, and (400) at 119.5° are extremely weak. This result indicates that (111)-oriented crystals are dominant in the film. A sharp peak at $2\theta=26.5°$ is due to a diffraction from graphite (002). It is seen that the intensity ratio of the graphite peak to the diamond (111) peak is smaller for the thicker diamond film. This fact suggests that the graphite exists in the vicinity of the interface between diamond and Pt.

Figures 19(a) and 19(b) are the results of polar XRD from a diamond film grown for 30 h on single-crystal Pt(111) [see

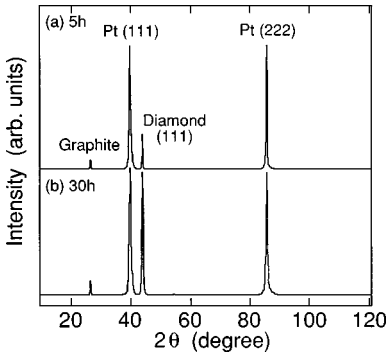

FIG. 18. XRD of diamond films grown for (a) 5 and (b) 30 h on bulk single-crystal Pt(111).

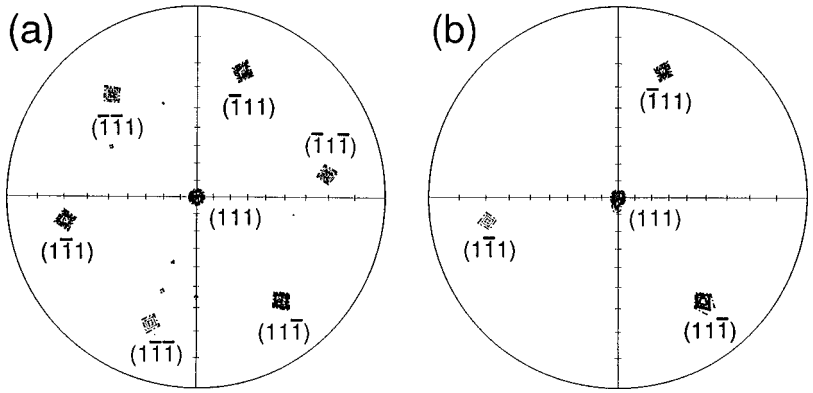

FIG. 19. X-ray pole figures of the {111} diffractions from (a) a diamond film grown for 30 h, and (b) the underlying bulk single-crystal Pt(111).

Fig. 15(a)] and the underlying Pt(111) substrate, respectively. Figure 19(a) shows that the diamond crystals in the film are (111)-oriented with respect to the tilt and azimuthal directions. The FWHM of the {111} diffraction poles is approximately 4°. This value is similar to the FWHM of highly (100)-oriented diamond films on silicon, i.e., 5°. However, it seems that the FWHM value for the diamond film includes diffraction signals from misoriented diamond particles near the Pt interface, because the top layer of Fig. 15(a) appears to have an almost perfect azimuthal alignment, as will be seen later in Fig. 22. Note that the coincidence of the diffraction patterns in Figs. 19(a) and 19(b) is evidence that the cubic crystal axes of the diamond film and the Pt substrate are parallel to each other.

In Fig. 19(a), it is of interest to note that (i) there are six {111} diffraction poles, rather than three, around the central (111) pole; and (ii) three diffraction poles [(111), (111), and (111)] are more intense that the other poles, [(111), (111), and (111)], though this may not be very apparent in the figure. Result (i) indicates that there are two possible orientations rotated by 60° in plane for the diamond crystals, which presumably correspond to the two equivalent sites on the Pt(111) surface, as illustrated in Fig. 20(a). A similar type of orientational structure is observed for β-SiC(111) epitaxially grown on 6H-SiC(0001).[40] In this case, incoherent boundaries, called double positioning boundaries, are formed in the film by 60°-rotated domains, as illustrated in Fig. 20(b). On the other hand, result (ii) indicates that the three orientations (111), (111), and (111) are preferable to the other orientations. The existence of nonequivalent diamond orientations on the cubic Pt(111) surface can be attributed to interactions with the second-nearest-neighbor Pt atoms. However, the ''incoherent boundaries'' due to the existence of 60°-rotated diamond crystals have not been identified yet. It is of great interest to note that recent preliminary growth experiments by the authors show that an azimuthally unidirectional surface is formed as the diamond CVD is continued for a longer time.

H. Interface between diamond and Pt

In order to study the interface between diamond and Pt, a diamond film of 9-μm thickness was delaminated from a bulk single crystal Pt(111), and the delaminated surfaces of both the diamond film and the substrate were observed by SEM. The micrographs are shown in Figs. 21(a) and 21(b). The Pt surface shown in Fig. 21(a) has a unique protrusive structure. By electron probe microanalysis, it was found that the protrusive structure was Pt and hence Fig. 21(a) indicates that the Pt intruded considerably into the diamond film. Later, in Sec. III J, it will be seen by TEM that Pt actually intruded into the diamond film along the grain boundaries near the interface. The reversed surface of the delaminated diamond film, shown in Fig. 21(b), was also very rough. The bright and dark contrast in the micrograph was produced by fragmented pieces of Pt that were firmly adhered to the diamond surface.

I. Planar TEM observation

Figure 22 shows a TEM image at the bottom of the diamond film where small and thin Pt remained to adhere to the

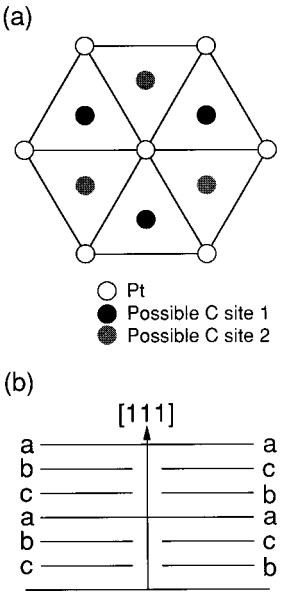

FIG. 20. Schematic diagrams showing (a) the two equivalent sites on the Pt(111) surface, and (b) the incoherent boundary between rotated domains.

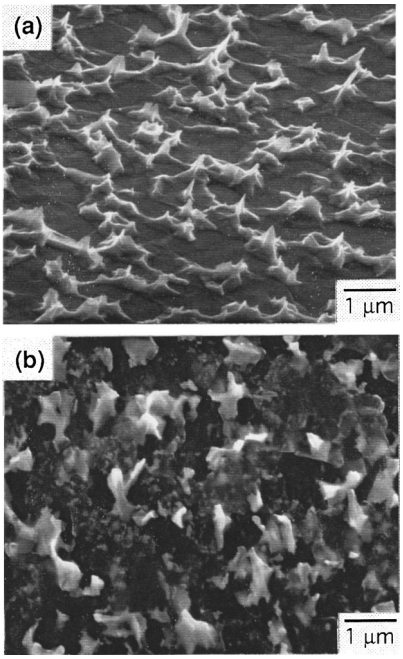

FIG. 21. SEM micrographs of (a) a delaminated surface of a bulk single-crystal Pt(111) substrate, and (b) a delaminated surface of a diamond film grown on the substrate.

film: the dark areas are Pt, while most of the transparent areas are diamond. The gray granular speckles are contaminants probably generated during the sample preparation. It is seen that most diamond crystals contain several types of defects: for example, the diamond crystals indicated by A and B in the figure contain diffraction contrasts due to internal defects. From the image contrast of equal thickness fringes, these defects are attributed to stacking faults. Crystal A appears to have grown on a small protrusion of Pt, indicative of direct nucleation on Pt. By contrast, crystal C in the figure has an elongate shape with fewer defects. Therefore, this diamond crystal is assumed to be a diamond fragmented during the ultrasonic treatment of the Pt substrate surface.

The inset in Fig. 22 shows a selected-area TED pattern of the same specimen. The number of rings in the interior part are due to Ga and Ga-Pt alloys generated during the TEM sample preparation process using Ga-ion FIB. The clear

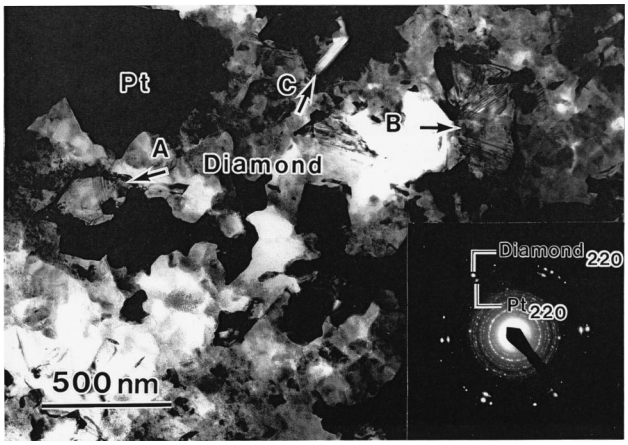

FIG. 22. Plan-view TEM micrograph of the bottom region, and the selected-area TED pattern.

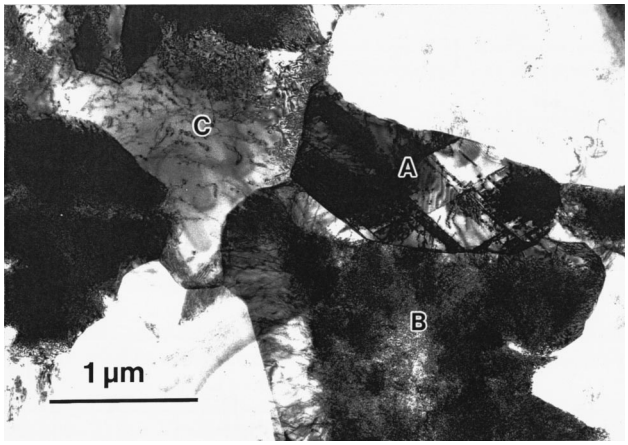

FIG. 23. Plan-view TEM micrograph of the middle region. Crystal A is oriented to ⟨110⟩, while crystals B and C are oriented to ⟨111⟩.

spots in the outer part are attributed to either crystalline Pt or diamond: the inner diffraction spots are assigned to Pt(220) with a lattice spacing of 0.139 nm, while the outer diffraction spots are assigned to diamond (220) with a lattice spacing of 0.126 nm. This TED pattern is clear evidence that some of the diamond crystals indeed grew epitaxially on Pt in such a way that the directions of the cubic axes of diamond agree with those of Pt. It should be noted that the diffraction spots of Pt are broad, indicating the existence of Pt that is slightly rotated about ⟨110⟩. The presence of the extra spots from diamond indicates that discretely rotated diamond crystals are also present.

Figure 23 shows a TEM image in the middle region of the film, where the film consists of diamond crystals of about 2 μm in size, many of them being well oriented in the ⟨111⟩ direction. The three crystals, indicated as A, B, and C in the figure, are typical diamond crystals existing in the region. Crystal A is oriented in the ⟨110⟩ direction, and includes both symmetric stacking faults created from the center of the crystal and a small number of dislocations. Crystal B is oriented in the ⟨111⟩ direction, and such crystals are most dominant in the specimen. This crystal has a high density of defects in the inner triangle area, while the outer skirt contains only a low density of dislocations. From the experimental data of the continuously rotated diffraction pattern and the minute diffraction contrast, it is inferred that the condensed defects in the inner part of crystal B consists of dense and tiny stacking faults with extra lattice planes, and that these defects have been created from a high density of point defects present during CVD, and then converted to stacking faults due to the internal stress in the cooling stage of the specimen after CVD. Crystal C also is oriented in the ⟨111⟩ direction, but contains a relatively low density of dislocations. This crystal has a complicated shape hampered by neighboring crystals, which indicates that crystal C grew later than the neighboring crystals. The defective area in crystal C seems to have been created due to large angle grain boundaries between the ⟨111⟩-directed crystal C and the adjacent ⟨110⟩-directed crystals.

A TEM image of the surface region is shown in Fig. 24. It consists of ⟨111⟩-directed diamond crystals of about 10 μm in size. It is noted that the defect density is smaller in the

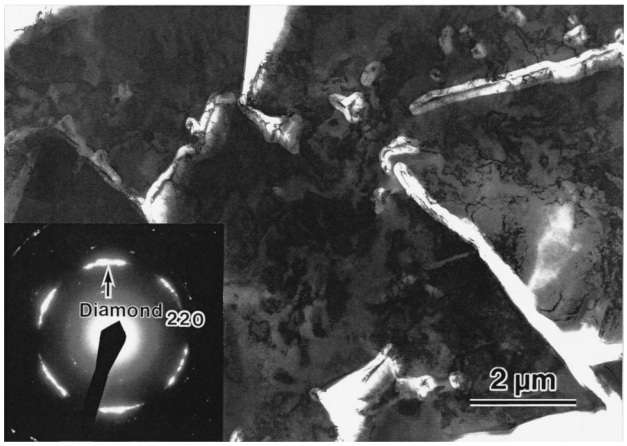

FIG. 24. Plan-view TEM and TED patterns of the surface region.

surface region than in the middle region shown in Fig. 23. Also, bright areas containing fewer defects exist at the grain boundaries, indicating that the misorientations between the adjacent crystals are very small. However, the TED pattern (see the inset), taken from the entire area shown in Fig. 19, has wide and continuous diffraction spots of $\pm 10°$. This indicates that the triangular crystals are not single crystal but consist of azimuthally rotated submicrostructures due to the coalescence of smaller diamond crystals.

The microstructures of the films observed by TEM are closely related to the time evolution of the film morphology shown in Sec. III D. The epitaxial relationship between diamond and Pt in the bottom region corresponds to the nucleation of oriented diamond particles with (111) faces seen in Figs. 9(a) and 9(b). The existence of high-density defects in the middle region (Fig. 23) can be a result of growth competition seen in Figs. 9(d) and 9(e). In the surface region, (111) faces are dominant, as seen in SEM (e.g., Fig. 15). The growth competition is restricted only at the grain boundaries, and as a consequence, the defect density in the (111)-oriented crystals is reduced.

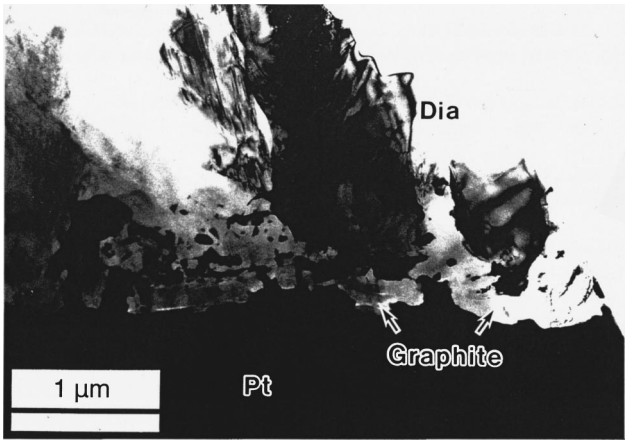

FIG. 25. Cross-sectional TEM image of the interface between diamond and Pt (low magnification).

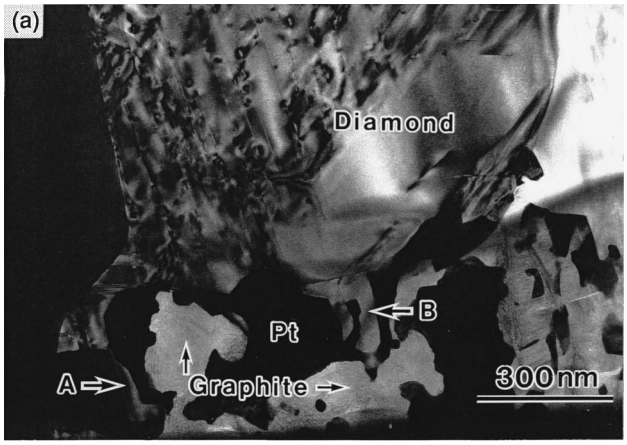

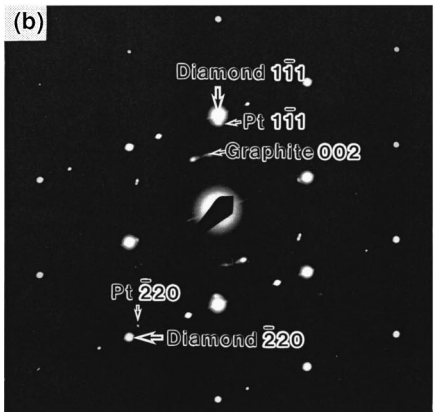

FIG. 26. (a) Cross-sectional TEM image and (b) selected-area TED pattern of the interface between diamond and Pt (high magnification).

J. Cross-sectional TEM observation

Figure 25 shows a low magnification cross-sectional TEM image of a diamond film grown on single crystal Pt film with a (111) surface. The upper part of this figure is diamond, while the bottom layer with a dark contrast is Pt. Discrete layers of graphite about 0.3 μm in thickness are also observed on the Pt. It is clearly seen that the diamond-Pt interface is extremely rough, even though it is found in Fig. 6(c) that the Pt surface is smoothed almost immediately after the exposure to CH_4/H_2 plasma. It is also observed that there are Pt particles trapped in the diamond region away from the Pt substrate.

Figure 26(a) is a magnified view of the diamond-Pt interface in Fig. 25. The transparent areas in the upper part of the figure are diamond, where the linear and spotty dark contrasts are stacking faults and separated dislocation loops, respectively. In the lower region, the dark areas are Pt, and the areas with a bright contrast are graphite surrounded by Pt. It is found that most diamond grains are directly in contact with Pt without any intermediate layer, and the interface is very rough. It is noteworthy that the diamond grains indicated by A and B in Fig. 26(a) have thin ''roots'' that intruded onto Pt. The intrude regions are free of defects as they have no diffraction contrasts.

Figure 26(b) is a selected-area TED pattern taken from the area of Fig. 26(a). The intense spots are from diamond,

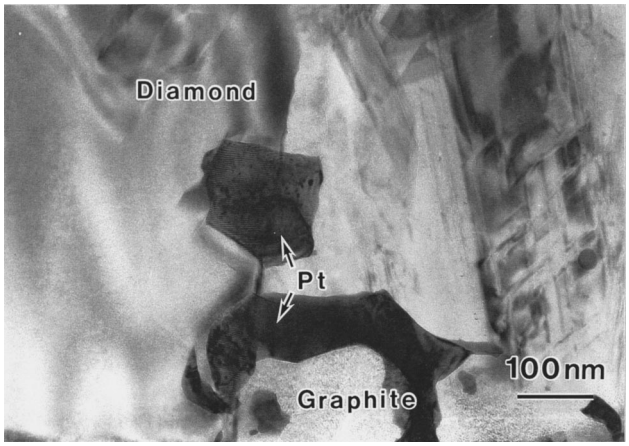

FIG. 27. Cross-sectional TEM image of the interface between diamond and Pt at the grain boundary of the diamond.

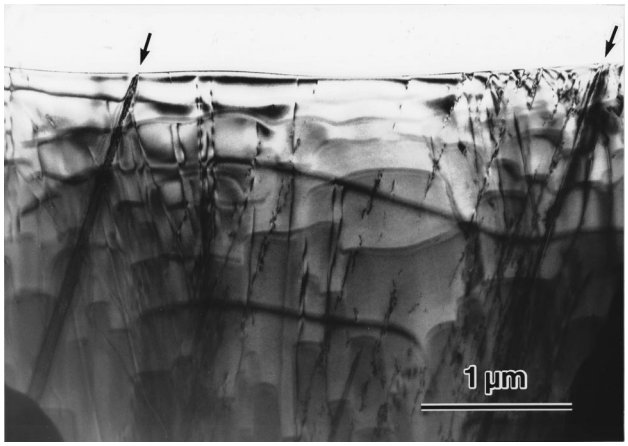

FIG. 28. Cross-sectional TEM image of a (111) grain at the surface.

while the small and weak spots right inside the intense spots are from Pt. Since the directions of the diffraction spots from diamond (111) and Pt(111) as well as from diamond (220) and Pt(220) agree, it is concluded that the diamond have grown epitaxially on the Pt substrate in the microscopic scale of TEM. In addition to the diffractions from diamond and Pt, it is noticed that rotated diffraction spots are present in the inner side, from which the lattice spacing was estimated to be about 0.35 nm. From this, it is concluded that graphite is present in the interface region, although the lattice spacing is 4% larger than that of standard graphite (002) (0.336 nm). It appears that the graphite is oriented parallel to the Pt surface, but not epitaxial to either diamond or Pt so that graphite does not seem to play an important role for epitaxial alignment of diamond. Figure 27 shows a TEM micrograph with a higher magnification of a different area near the diamond-Pt boundary in Fig. 25. It is seen that a small Pt particle is trapped at a diamond grain boundary. There is an overlap of Pt on diamond on the left-hand side of the Pt particle, where more fringes are seen along the Pt-diamond interface. This clearly indicates that the diamond and the Pt are epitaxially aligned.

As seen in Figs. 25–27, the interface between diamond and Pt, which is supposed to be originated during the nucleation and growth stages, is extremely intricate. This intricate interface structure observed by TEM is consistent with the results of SEM micrograph in Fig. 21, where the protrusion of Pt into diamond is seen. The following two possibilities for the intricate interface formation are considered: the first is that the residual diamond particles, embedded in the Pt surface layer during the ultrasonic treatment, became the nuclei for diamond film formation. Indeed, the existence of such diamond particles is observed by XRD (Fig. 5). Furthermore, the diamond crystals intruded onto Pt have only a very low defect density, as seen in Fig. 26(a), suggesting that they are different from diamond created by CVD; the second is that diamond nuclei are formed from the Pt-C-H complex as described in Sec. III C. The arguments supporting this possibility have been given in Ref. 26. Furthermore, the intruded diamond crystals have a wavy form at the interface, as crystal B in Fig. 26(a), which indicates that they were partially dissolved into Pt. It is of great interest that diamond and Pt are in an epitaxial relationship even though the interface has an intricate structure.

The graphite detected by XRD (Fig. 18) seems to exist at the film-substrate interface, as shown in Fig. 26. Since the lattice structure as well as the interatomic distance of diamond (111) plane is similar to that of the basal plane of graphite, it may be considered that a single-crystal graphite has been formed in precedence to diamond growth. In fact, such a model is proposed in Ref. 41. However, the TEM results in Figs. 26 and 27 show that the graphite is epitaxial to neither diamond nor Pt, hence eliminating this possibility. Therefore, it is concluded that the graphite existing at the Pt-diamond interface area is only a side product due to a reaction between diamond and Pt or due to the Pt-C-H complex formed in Pt immersed in CH_4/H_2 plasma, as inferred from the binary phase diagram.[25] This view is consistent with the observed fact that the graphite at the interface area is usually enclosed with a Pt layer, as seen in Fig. 27.

Figure 28 is a cross-sectional TEM image of a diamond section vertically carved out of the center of a (111) crystal at the surface of about 10-μm-thick diamond film grown on a (111) domain of the specially processed Pt foil. It is remarkable that the defect density in the central area of the diamond crystal is as low as 10^8 cm^2. This value is comparable to those in homoepitaxial diamond films. The arrows in Fig. 28 indicate small-angle grain boundaries between the adjacent diamond crystals. The weak TEM contrast indicates that the adjacent diamond crystals have only a small misalignment of less than 0.01°. This result indicated the possibility that single crystal diamond film with a low density of defects can be grown, if the coalescence is developed further by CVD.

IV. PROCESS OF ORIENTED GROWTH

The experimental results and discussion presented so far are diagramatically summarized in Fig. 29: (1) diamond crystals are embedded in the rough Pt surface during the ultrasonic treatment, (2) the diamond crystals undergo positional and orientational changes to align epitaxially at the molten Pt surface, and (3) they partially dissolve in Pt to form a Pt-C-H complex. On the other hand, (4) the CH_4/H_2 plasma forms a Pt-C-H complex which then contributes diamond nucleation, and (5) the plasma smooths the Pt surface to recover the (111) structure; (6) most of these nuclei are

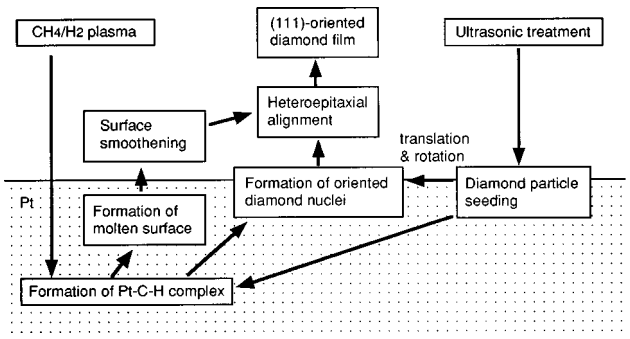

FIG. 29. A summary diagram for heteroepitaxial growth processes of (111)-oriented diamond film on Pt(111).

epitaxially oriented with respect to the Pt lattice, and the (111) textured growth of diamond occurs as a result of the growth competition; finally, (7) spontaneous coalescence of (111) faces takes place. It remains to be investigated more closely whether this model is actually the case.

V. CONCLUSION

It is shown that highly oriented and spontaneously coalesced diamond films with (111) crystal faces were grown by microwave plasma chemical vapor deposition (CVD) on single-crystal Pt(111) domains or surfaces that had been scratched by buff polishing and ultrasonic treatment. The most intriguing phenomenon is the fact that the (111) faces are azimuthally oriented and that the coalescence of (111) faces of diamond grains took place spontaneously, even though the initial substrate surface was roughened due to the scratching. It was found that the roughened surface was smoothed by H_2 or CH_4/H_2 plasma within 1 min, presumably because the Pt surface was molten due to the exposure plasma at high temperature (875 °C). The nucleation density of diamond was about 4×10^7 cm^{-2} by buff polishing, while it was about 7×10^8 cm^{-2} by the ultrasonic treatment. This fact, along with the XRD results, suggests that diamond particles fragmented during the ultrasonic treatment were embedded in the Pt surface layer to be the seeds for diamond nucleation. SEM observation of the growth process shows that small diamond particles at the Pt surface underwent positional and orientational changes due to the molten state of the Pt surface. The diamond growth at a later stage was governed by the van der Drift mechanism to form an azimuthally oriented (111) faces.

The epitaxial relationship between diamond and Pt was confirmed by polar XRD and TEM. In particular, it was discovered by TEM that the Pt-diamond film interface has an intricate structure, including Pt, diamond, and graphite. Such a structure seems to have occurred as the result of a Pt-C-H formation in the Pt surface layer. The appearance of oriented diamond crystals partially embedded in Pt seems to be evidence of the complex formation.

The (111)-oriented crystal at the film surface was found to have a remarkably low defect density of 10^8/cm^2, comparable to those in homoepitaxial diamond films. These results suggest the possibility of growing completely coalesced diamond films with a very low density of defects by CVD.

The nucleation and growth features followed by a spontaneous coalescence of diamond faces observed in the present paper are unprecedented, and clearly indicate the existence of an interesting mechanism of heteroepitaxy. It is therefore expected that heteroepitaxial growth on relatively inactive metals such as Pt will be found for other covalently bonded materials, if proper metallic substrates are identified.

[1] Y. Shintani, J. Mater. Res. **11**, 2955 (1996).
[2] T. Tachibana, Y. Yokota, K. Nishimura, K. Miyata, K. Kobashi, and Y. Shintani, Diamond Relat. Mater. **5**, 197 (1996).
[3] M. Kamo, S. Matsumoto, Y. Sato, and N. Setaka, US Patent No. 4,434,188 (28 February 1984).
[4] S. Koizumi, T. Inuzuka, T. Inuzuka, and K. Suzuki, Appl. Phys. Lett. **57**, 563 (1990).
[5] M. Yoshikawa, H. Ishida, A. Ishitani, S. Koizumi, and T. Inuzuka, Appl. Phys. Lett. **58**, 1387 (1991).
[6] B. R. Stoner and J. T. Glass, Appl. Phys. Lett. **60**, 698 (1992).
[7] S. Yugo, T. Kanai, T. Kimura, and T. Muto, Appl. Phys. Lett. **58**, 1036 (1991).
[8] H. Kawarada, T. Suesada, and H. Nagasawa, Appl. Phys. Lett. **66**, 583 (1995).
[9] X. Jiang and C.-P. Klages, Diamond Relat. Mater. **2**, 1112 (1993).
[10] B. R. Stoner, S. Sahaida, J. P. Bade, P. Southworth, and P. J. Ellis, J. Mater. Res. **8**, 1334 (1993).
[11] T. Tachibana, K. Hayashi, and K. Kobashi, Appl. Phys. Lett. **68**, 1491 (1996).
[12] M. Schreck, R. Hessmer, S. Geier, B. Rauschenbach, and B. Stritzker, Diamond Relat. Mater. **3**, 510 (1994).
[13] Y. Sato, I. Yashima, H. Fujita, T. Ando, and M. Kamo, in *Proceedings of the Second International Conference on New Diamond Science and Technology*, edited by R. Messier, J. T. Glass, J. E. Butler, and R. Roy (Materials Research Society, Pittsburgh, 1991), p. 371.
[14] P. C. Yang, W. Zhu, and J. T. Glass, J. Mater. Res. **8**, 1773 (1993).
[15] W. Liu, D. A. Tucker, P. Yang, and J. T. Glass, J. Appl. Phys. **78**, 1291 (1995).
[16] S. J. Harris, D. N. Belton, A. M. Weiner, and S. J. Schmeig, J. Appl. Phys. **66**, 5353 (1989).
[17] D. N. Belton and S. J. Schmeig, Surf. Sci. **233**, 131 (1990).
[18] D. N. Belton and S. J. Schmeig, J. Appl. Phys. **69**, 3032 (1991).
[19] M. Takaya and Y. Sakamoto, in *First International Conference on Processing Materials for Properties*, edited by H. Henein and T. Oki (Minerals, Metals & Materials Society, Warrendale, PA, 1993), p. 1157.
[20] Y. Yokota, T. Tachibana, K. Miyata, K. Kobashi, and Y. Shintani, Diamond Films Technol. **6**, 165 (1996).
[21] M. Tarutani, Y. Takai, R. Shimizu, K. Uda, and H. Takahashi, Technol. Rep. Osaka Univ. **43**, 167 (1993).
[22] S. Iijima, Y. Aikawa, and K. Baba, J. Mater. Res. **6**, 1491 (1991).
[23] T. Ishikura, S. Yamashita, S. Ojika, and H. Kawarada, in *Advances in New Diamond Science and Technology*, edited by S. Saito, N. Fujimori, O. Fukunaga, M. Kamo, K. Kobashi, and M. Yoshikawa (MYU, Tokyo, 1994), p. 283.
[24] H. Reiss, J. Appl. Phys. **39**, 5045 (1968).

[25] *Binary Alloy Phase Diagrams*, 2nd ed., edited by T. B. Massalski (ASM, Materials Park, Ohio, 1990), p. 873.
[26] R. Roy, H. S. Dewan, and P. Ravindranathan, Mater. Res. Bull. **28**, 861 (1993).
[27] A. van der Drift, Philips Res. Rep. **22**, 267 (1967).
[28] K. Kobashi, K. Nishimura, Y. Kawate, and T. Horiuchi, Phys. Rev. B **38**, 4067 (1988).
[29] Ch. Wild, N. Herres, and P. Koidl, J. Appl. Phys. **66**, 973 (1990).
[30] S. Barrat and E. Bauer-Grosse, Diamond Relat. Mater. **4**, 419 (1995).
[31] W. Zhu, P. C. Yang, J. T. Glass, and F. Arezzo, J. Mater. Res. **10**, 1455 (1995).
[32] H. Boppart, J. van Straaten, and I. F. Silvera, Phys. Rev. B **32**, 1423 (1985).
[33] W. F. Sherman, J. Phys. C **18**, L973 (1985).
[34] S. K. Sharma, H. K. Mao, P. M. Bell, and J. A. Xu, J. Raman Spectrosc. **16**, 350 (1985).
[35] P. K. Bachmann and D. U. Wiechert, Diamond Relat. Mater. **1**, 422 (1992).
[36] S. K. Choi, D. Y. Jung, and H. M. Choi, J. Vac. Sci. Technol. A **14**, 165 (1996).
[37] D. Rats, L. Bimbault, L. Vandenbulcke, R. Herbin, and K. F. Badawi, J. Appl. Phys. **78**, 4994 (1995).
[38] M. H. Grimsditch, E. Anastassakis, and M. Cardona, Phys. Rev. B **18**, 901 (1978).
[39] M. Hanfland, K. Syassen, S. Fahy, S. G. Louie, and M. L. Cohen, Physica B&C **139/140B**, 516 (1986).
[40] H. S. Kong, B. L. Jiang, J. T. Glass, G. A. Rozgoni, and K. L. More, J. Appl. Phys. **63**, 2645 (1988).
[41] W. R. L. Lambrecht, C. H. Lee, B. Segal, J. C. Angus, Z. Li, and M. Sunkara, Nature (London) **364**, 607 (1993).